Homography-based change detection for space based satellite inspection

Ryan L. Buffington[a] and John E. McInroy[a]

[a]Electrical and Computer Engineering Department, University of Wyoming,
1000 E. University Ave., Laramie, WY USA 82071

ABSTRACT

In order to maintain space situational awareness, it is necessary to maintain surveillance of objects in Earth orbit. A system of space-based imaging sensors could make much more detailed inspections of the existing resident space objects (RSOs). However, in order to preserve bandwidth, it is desirable to send the groundstation only a subset of all images which are taken by the inspection system. This paper presents a change detection algorithm which can detect changes in the appearance of an RSO. A new inspection image is compared to a previously taken base image. In each image, the translation vector and rotation matrix between the camera and the RSO, or pose, is slightly different. Assuming that the points making up each image of the RSO are within a single plane, it is possible to generate a planar homography which is a linear mapping between the two images. The homography is used to estimate the rotation and translation between the camera coordinate systems. This knowledge can be used to warp the inspection image so that it appears as though it was taken from the same coordinate system as the base image. Finally, basic morphological image processing and image thresholding techniques are used to perform change detection. The algorithm was evaluated by applying it to raytraced inspection images exhibiting varying lighting and pose conditions. Simulation results show that the algorithm can reliably detect damage to the RSO or the rendezvous of a suspicious object.

Keywords: change detection, planar homography, homography estimation, satellite inspection, morphological image processing

1. INTRODUCTION

Space situational awareness (SSA) is the act of knowing the location of every object in orbit of the earth, the purpose of each object, and where each object will be in the future.[1] The objects which are subject to inspection are denoted resident space objects (RSOs). These objects can include any object in orbit, including satellites, space debris, or natural objects. Military satellite operators need to be able to perform routine inspections of friendly satellites for damage. They must also be able to inspect satellites which have failed, so that the cause of failure may be determined. Inspecting the RSOs launched by other parties would allow the identification of hostile satellites so that appropriate countermeasures can be implemented.

Orbiting inspection satellites have several advantages over ground-based surveillance systems. Ground-based telescopes can only operate at night and can not operate through cloud cover.[1] Ground-based radar systems require tremendous power to characterize objects in GEO due to the distance between the Earth and GEO.

Inspection satellites would be much closer to the RSOs and therefore would require simpler optics with smaller apertures. Inspection satellites do not have to cope with the degradation introduced by the atmosphere. They can perform surveillance above regions that ground-based systems can not be placed, such as over hostile territory or the ocean. A distributed network of inspection satellites may be more resistant to attack by an adversary than a ground-based system.

Change detection is a field within computer vision which has been studied extensively. In change detection, two or more images taken at different times are compared to determine if an object of interest has been added or removed from a scene. For example, change detection has been used to detect suspicious people or packages as

Send correspondence to mcinroy@uwyo.edu

Sensors and Systems for Space Applications IV, edited by Khanh D. Pham, Henry Zmuda,
Joseph Lee Cox, Greg J. Meyer, Proc. of SPIE Vol. 8044, 804409 · © 2011 SPIE
CCC code: 0277-786X/11/$18 · doi: 10.1117/12.884086

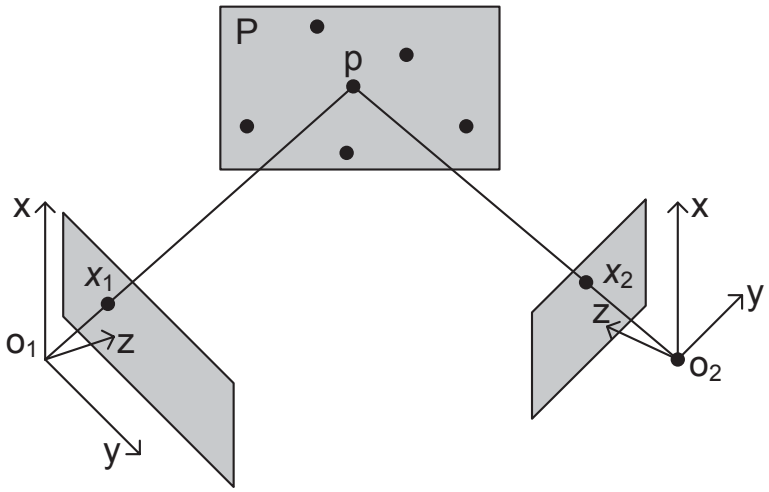

Figure 1. Dual view geometry

they appear in surveillance videos of public areas, and it has been used to detect vehicles in traffic surveillance videos.

Change detection has applications in space-based inspection systems due to the relatively low bandwidth of the communications links between the inspection satellites and the ground. In order to conserve bandwidth, it is desirable to have the inspection satellite take many images but only transmit the subset of images which contain new information. A change detection algorithm could be used to detect visual changes to an RSO. Images containing changes could be flagged for transmission to human operators on the ground. Such an algorithm would detect damage to the exterior of the RSO. It could also be used to detect unauthorized objects which are following or have docked with the RSO.

2. THEORETICAL BACKGROUND

2.1 Dual view geometry

Assuming that two images of the same scene are generated with the ideal perspective camera model,[2] it is possible to relate the images mathematically. For example, in Figure 1, two images of point p were taken by two cameras. One camera was located at o_1 and the other at o_2. Point p can be expressed in either of the camera coordinate systems, as shown in Equation 1, where X_1 is point p in coordinate system $\{o_1\}$, and X_2 is p in system $\{o_2\}$. The matrix R_{21} is the rotation matrix from $\{o_1\}$ to $\{o_2\}$, and vector T_{21} is the translation vector from the origin of $\{o_1\}$ to the origin of $\{o_2\}$, expressed in $\{o_2\}$.

$$X_2 = R_{21}X_1 + T_{21} \tag{1}$$

When an image is captured using a single camera, the information about the depths of points in the scene is lost. If two images of the scene from different camera positions are available, it is possible to reconstruct the depths of the points in the scene. Stereo reconstruction algorithms use the image plane positions of a group of points to estimate the rotation, R, and translation, T, between the two camera systems. These algorithms also produce the locations of these points in 3D space.

To determine the relationship between two camera systems, it is necessary to have a set of image plane points which correspond to the same points in 3D space. Let p_i, $i = 1, 2, \ldots n$, be n points in the world which have images x_1^i in the first image plane and images x_2^i in the second image plane, as shown in Figure 1. Then the pairs of image plane points x_1^i, x_2^i are called correspondence points.

Finding correspondence points in real images is an active area of research in the computer vision community. One simple method of finding correspondence points is to use fiducial markers such as a lights on the corners of

the object or a specially designed high contrast pattern painted on the object. Unfortunately, the use of fiducial markers does not work unless the objects have distinct, unambiguous features that are easy to recognize. Another method proposed by Lowe is the Scale-Invariant Feature Transform (SIFT).[3] This transform automatically generates correspondence points by performing calculations on each point and its neighboring pixels.

2.2 Planar Homography

Assume that there are many points in the image which all reside in plane P in Figure 1. For these points on plane P, it is possible to simplify Equation 1 into the linear mapping in Equation 2. This mapping is referred to as a planar homography.[2] Equation 3 defines the planar homography matrix H, where N is the unit normal of plane P in coordinate system $\{o_1\}$, and d is the distance from plane P to o_1.

$$X_2 = HX_1 \tag{2}$$

$$H \equiv R + \frac{1}{d}TN^T \in \mathbb{R}^{3\times 3} \tag{3}$$

The cross product matrix of vector a is denoted by $\hat{a}$, so that $a \times b \equiv \hat{a}b$. For $a \in \mathbb{R}^3$, $\hat{a}$ is given by Equation 4.

$$a = \begin{bmatrix} a_1 \\ a_2 \\ a_3 \end{bmatrix} \in \mathbb{R}^3, \quad \hat{a} = \begin{bmatrix} 0 & -a_3 & a_2 \\ a_3 & 0 & -a_1 \\ -a_2 & a_1 & 0 \end{bmatrix} \in \mathbb{R}^{3\times 3} \tag{4}$$

Since $\hat{\mathbf{X}}_2\mathbf{X}_2 = \mathbf{X}_2 \times \mathbf{X}_2 = 0$, Equation 2 can be rewritten as $\hat{\mathbf{X}}_2 H \mathbf{X}_1 = 0$. Application of the ideal calibrated perspective transform produces the planar epipolar constraint in Equation 5.

$$\hat{\mathbf{x}}_2 H \mathbf{x}_1 = 0 \tag{5}$$

Many algorithms for estimating the homography between two different camera systems have been developed. One such algorithm is Algorithm 1, the four-point homography algorithm.[2] This algorithm generates H so that the planar epipolar constraint is maintained for a set of at least four pairs of correspondence points on the plane.

One simple measure which can be used to estimate the accuracy of a reconstruction algorithm is the reprojection error. Reprojection error measures the difference in image plane position between each correspondence point and the reprojected correspondence point from the other image. The reprojected correspondence point is generated by using the reconstruction model to project the point from the other image. The reprojection error is calculated using Equation 6, where $\tilde{x}_1^i$ and $\tilde{x}_2^i$ are the predicted image plane positions of correspondence point i in image I_1 or I_2, respectively.

$$\sum_i |\tilde{x}_1^i - x_1^i|^2 + |\tilde{x}_2^i - x_2^i|^2 \tag{6}$$

For homography algorithms, the points x_1^i and x_2^i are found using the planar homography mapping $x_2 \sim Hx_1$, where $\sim$ denotes equality up to a scale factor. This produces the result in Equation 7. To ensure that the results are in homogeneous coordinates, it is necessary to normalize the resulting x_1^i and x_2^i so that each z-value is 1.

$$\tilde{x}_2^i \sim Hx_1^i, \quad \tilde{x}_1^i \sim H^{-1}x_2^i \tag{7}$$

3. METHOD

The homography-based change detector takes two inspection images of an RSO and identifies areas of the RSO where its visible appearance is not the same in both images. The first image, or base image, is denoted I_1 and is taken from the coordinate system $\{o_1\}$. The second image, or comparison image, is taken from a different location after a period of time has elapsed. The comparison image is denoted I_2 and is taken from system $\{o_2\}$. The combination of position and orientation between the camera and RSO is called the pose of a given scene. Since images I_1 and I_2 contain different poses, it is not possible to compare the images without adjusting for these differences.

Satellites frequently contain highly planar surfaces, such as solar arrays. In addition, the distance between the camera and the RSO is much larger than the distances in the relief of the RSO. Therefore, it is possible to simplify the multiple view geometry of the image by assuming that all of the visible points on a RSO lay in a single plane. This permits the use of the planar homography geometry developed in Section 2.2. The homography-based change detector generates a homography, H, between I_1 and I_2. The linear mapping described by H is used to warp I_1 so that it appears as though it was taken from $\{o_2\}$. Image subtraction and thresholding are used to perform change detection. Finally, a morphological filter is used to smooth out the homography estimation error.

3.1 Homography Generation

The planar homography is calculated using Algorithm 1, the four point homography algorithm. This algorithm requires a minimum of four pairs of correspondence points to estimate H. This algorithm attempts to find a H matrix which solves Equation 5 for each pair of points. The Kronecker product and singular value decomposition are used to minimize $\hat{x}_2^i H x_1^i$ over the correspondence points $i = 1, 2, \ldots, n$. This produces a stacked version of the homography matrix, as given in Equation 8. Since well-formed homography matrices have a second singular value which is equal to one, the unstacked version of the homography matrix, H_L, is normalized by dividing it by its second singular value.

$$H_L^s \equiv \begin{bmatrix} h_1 \\ h_2 \\ h_3 \end{bmatrix} \in \mathbb{R}^9, \quad H_L = \begin{bmatrix} h_1 & h_2 & h_3 \end{bmatrix} \in \mathbb{R}^{3\times 3} \tag{8}$$

Algorithm 1 The four point planar homography algorithm

Given a set of n image correspondence points x_1^i, x_2^i, for $i = 1, 2, \ldots, n$, and $n \geq 4$, such that all 3-dimensional points X are on the same plane $N^T X = d$, this algorithm estimates the planar homography matrix H where $X_2 = HX_1$.

1. The χ vector is generated by assembling the vectors $a^i = x_1^i \otimes \hat{x}_2^i$ into the matrix $\chi = \begin{bmatrix} a^1, a^2, \ldots, a^n \end{bmatrix}^T$, $\chi \in \mathbb{R}^{3n\times 9}$.
2. The homography matrix is estimated by taking the singular value decomposition of χ to get $\chi = U\Sigma V^*$. H_L^S is the ninth column of matrix V. The vector H_L^S is unstacked into the matrix $H_L \in \mathbb{R}^{3\times 3}$.
3. H_L is divided by its second singular value to produce H.

Correspondence points may be automatically generated using the scale-invariant feature transform (SIFT). The VLFeat toolbox[4] was used to compute the SIFT descriptors for each of the two images. Next the `vl_ubcmatch` function was used to match the sets of SIFT descriptors into correspondence point pairs. The function returns pairs of image plane positions which are associated with the same point on the object. The function eliminates any poor matches or descriptors that are not present in the other image using Lowe's method.[3] This step produces approximately 30–50 correspondence point pairs for each pair of images.

3.2 Image Warping

The homography matrix, H, maps the location of image points in systems $\{o_1\}$ and $\{o_2\}$ as given in Equation 7. Modifying this equation to account for scaling produces Equation 9. The location of the points in I_1 are shifted from their old locations x_1 to new locations Hx_1, which warps I_1 so that it is from the same viewpoint as I_2. This third image is called the warped image, I_w.

$$x_2 = \frac{Hx_1}{z^T Hx_1} \tag{9}$$

Some pixels in I_1 may map to a location in $\{o_2\}$ that is outside the visible area. These pixel values are discarded. Similarly, not all pixels in the visible area of $\{o_2\}$ may have a corresponding I_1 value. These locations are filled with black pixels. Some form of interpolation must used when the pixels in the original image and the warped image do not form a one-to-one match.

3.3 Morphological Filtering and Thresholding

Change detection is performed between the comparison image I_2 and the warped image I_w. A difference image is generated by taking the absolute value of the difference of I_2 and I_w.

Mismatches along the edges of the RSO are common at this stage. These can be created by minor errors in the homography estimate, such as those caused by noise in the correspondence points. They are also caused by image occlusions, such as when one side of the RSO is visible in I_2 but not I_1. Errors are also introduced by the assumption that all points lay on a single plane. Points that are not on this plane are subject to warping errors which are proportional to their distance from the homography plane.

Since these mismatches are long and thin, they are a good candidate for removal using morphological filtering. The morphological erosion operator is used to remove any errors which do not satisfy a minimum thickness requirement. A ball-shaped structuring element with a radius of five to eight pixels was used with success. Larger structuring elements are more aggressive at removing homography errors, but have the potential to generate false negatives.

The image was thresholded to convert it to a binary image. The gray level threshold was selected using Otsu's method.[5] Otsu's method is an optimal algorithm which operates on the histogram of the image to minimize the between-class variance of the the black and white values in the black and white image. This final image highlights areas where change has been detected using white pixels.

4. SIMULATION

To evaluate the performance of this algorithm, it was tested using computer-generated images of satellites in orbit. The majority of the testing was accomplished using a 3D model of the Aura satellite.[6] The Aura spacecraft is made up of a main body covered in gold foil with a single large solar array to the side. This spacecraft was selected for use in these simulations due to its combination of a nearly planar surface (the solar array) and nonplanar surfaces (the spacecraft body and antennas). A small, gray box with beveled edges was placed on the spacecraft body to test the algorithm's ability to detect its removal.

To determine the importance of accurate image correspondence points, testing was performed using correspondence points selected by hand and correspondence points generated using the SIFT. The images which were used to test the algorithm are presented in Figure 2. Note that each image has a slightly different pose, and that the gray box attached to the upper right corner of the RSO in I_1 has been removed in I_2. This simulates an RSO which has suffered damage in the time that elapsed between the two images.

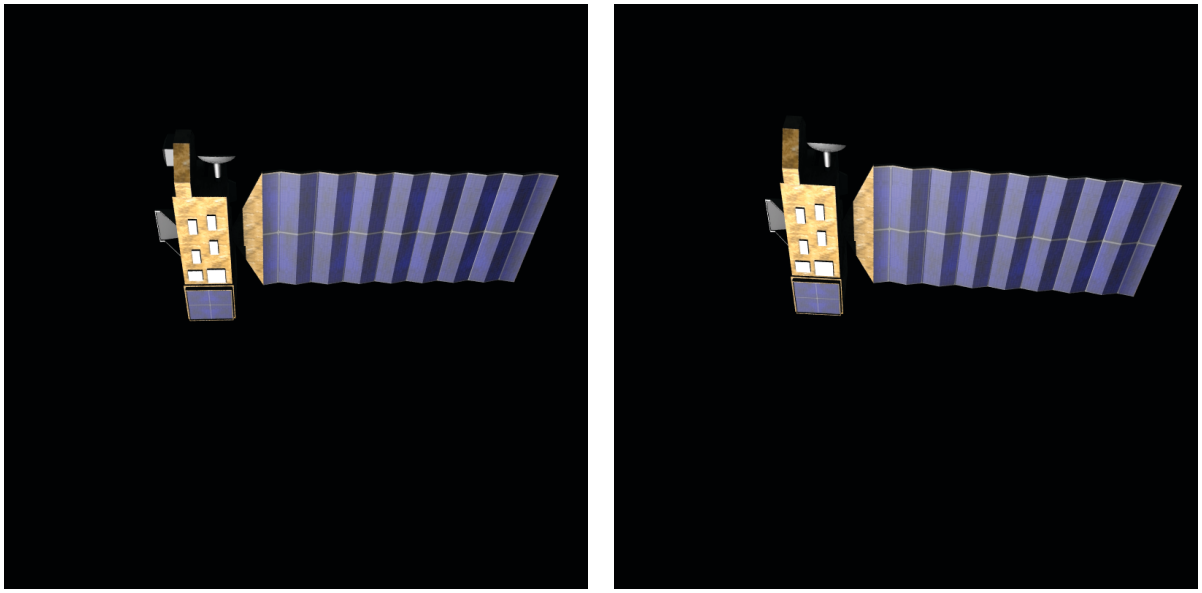

(a) Base inspection image I_1 (b) Comparison inspection image I_2

Figure 2. Test images

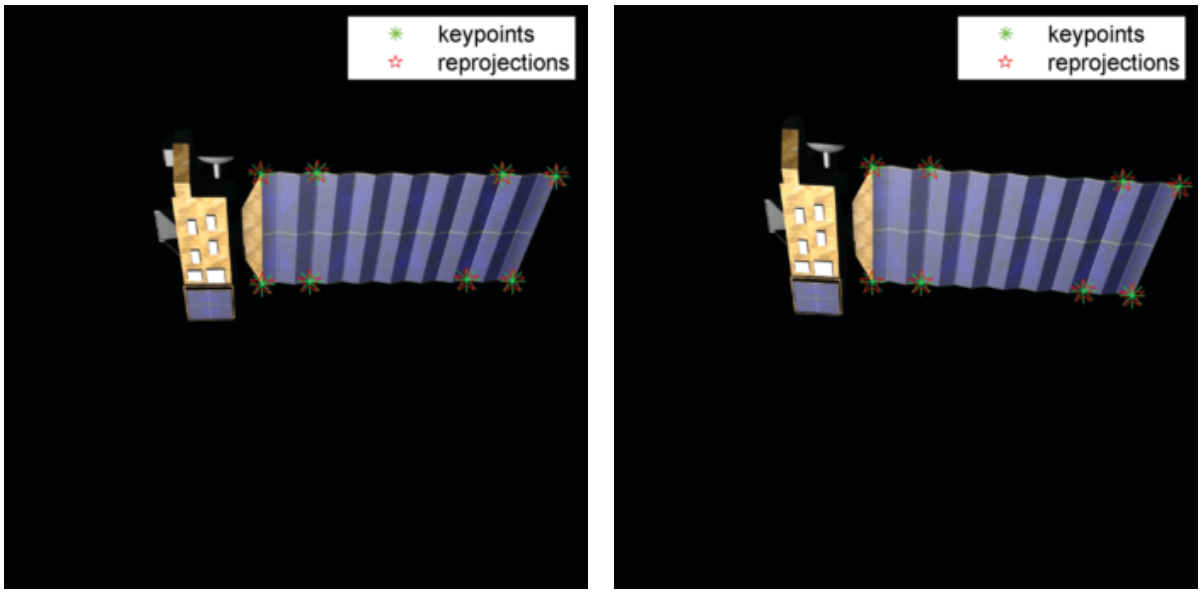

(a) Base image correspondence points (b) Comparison image correspondence points

Figure 3. Manual correspondence points

4.1 Manual Correspondence Points

To ensure accuracy, the image correspondence points used to estimate the homography between the images were selected by hand. These correspondence points are shown as green asterisks in Figure 3. The majority of the correspondence points were placed on the solar array, which is nearly planar. This produces the best estimate of the actual homography.

In order to estimate the accuracy of the homography, the image correspondence points were reprojected using Equation 7. These reprojections are denoted by the red stars in Figure 3. As expressed in Equation 6, a good homography estimate will produce reprojections which are close to their measured correspondence points.

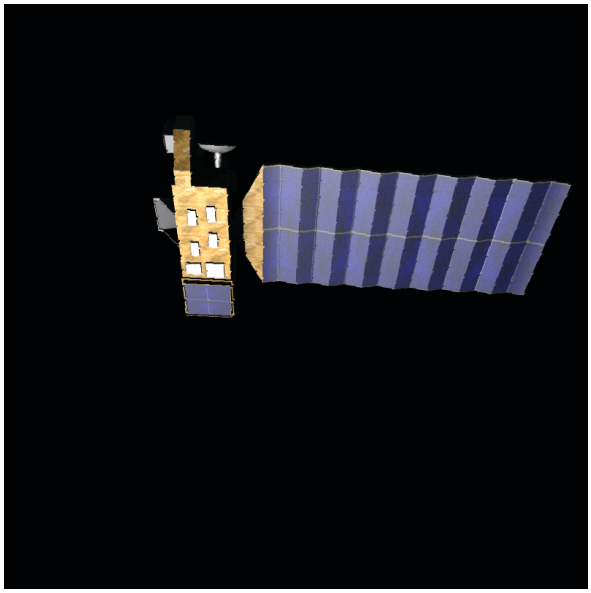

Figure 4. Warped image

The result of warping I_1 to the viewpoint of I_2 is shown in Figure 4. Note that the box is present in this image, since it was present in I_1.

The result of directly subtracting I_1 and I_2 is given in Figure 5(a). The change in pose was not taken into account, as no homography estimation or warping were used. As a result, the pose differences between these two images have been identified as changes in regions of the satellite which did not change. This simplified method is not sufficient for cases where even minor changes in pose may occur.

Compare this to the result in Figure 5(b) obtained by subtracting the warped version of I_1 and an unmodified version of I_2. This difference image has detected very little change along the solar array where the estimate of the homography is the most accurate. Changes have been detected along the antenna and the edges of the spacecraft body, since these edges do not lay in the same plane as the correspondence points. Recall that the warping error for points not in the homography plane is proportional to the distance between the point and the plane.

The thin nature of these errors makes it trivial to find and remove them using morphological filtering. A morphological erosion filter utilizing a ball-shaped structuring element with a radius of five pixels was applied to the image in Figure 5(b). This produced the eroded difference image in Figure 6(a). Finally, the eroded difference image was converted to a binary image using Otsu's method. This produced the change detection result in Figure 6(b). Regions where change has been detected are denoted as white in this image. The homography-based change detection algorithm has successfully flagged the absence of the gray box on the upper right corner of the RSO.

4.2 Automatic Correspondence Points

The same images used in the previous section were processed using automatically generated correspondence points. The correspondence points were selected automatically using the Scale Invariant Feature Transform. For the pair of images in Figure 2, approximately 140 SIFT features were found in each image. Of these features, 40 were determined to be correspondence points using Lowe's algorithm. These correspondence points are shown in Figure 7.

The correspondence points were used to generate a homography estimate using Algorithm 1. This homography estimate produced the reprojections given in Figure 8. Note that due to the noise in the correspondence points, and due to the increased number of correspondence points which do not reside on the homography plane, these reprojections are not as accurate as those in Figure 3.

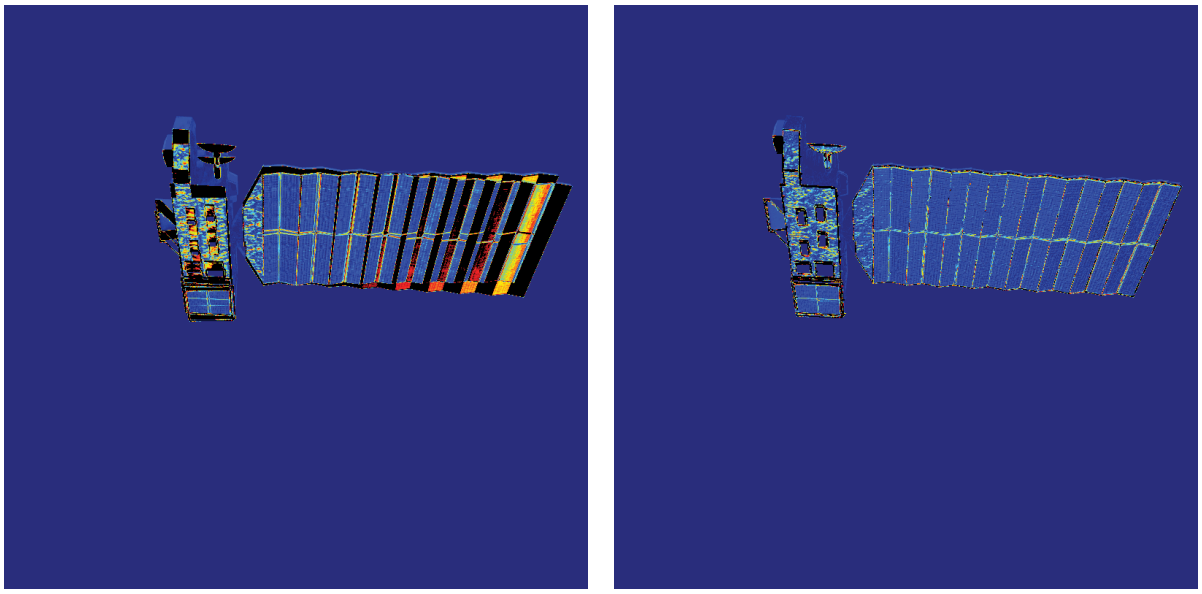

(a) Direct difference image $I_1 - I_2$ (b) Warped difference image

Figure 5. Comparison of difference images

(a) Eroded warped difference image (b) Change detection result

Figure 6. Removal of homography errors

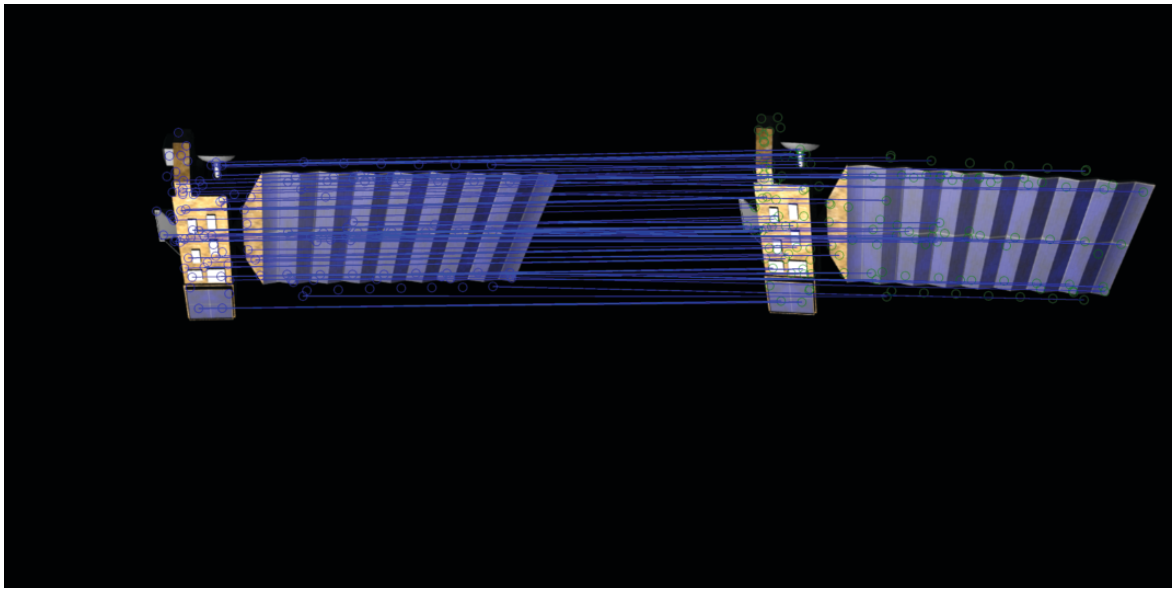

Figure 7. Correspondence points found using SIFT

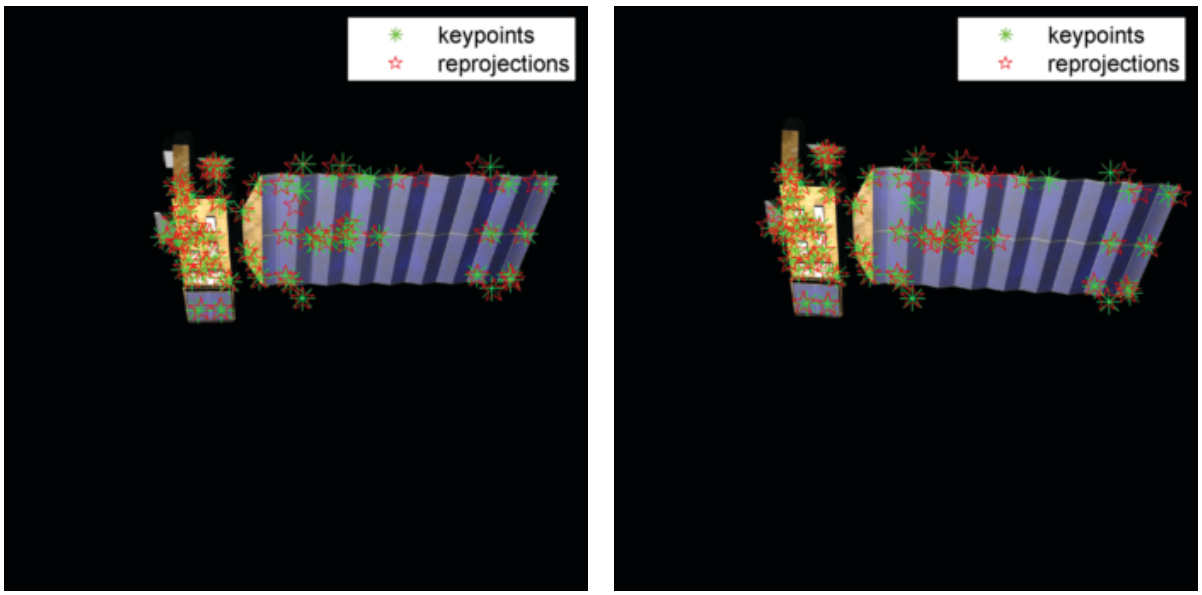

(a) Base image correspondence points (b) Comparison image correspondence points

Figure 8. Automatic correspondence points

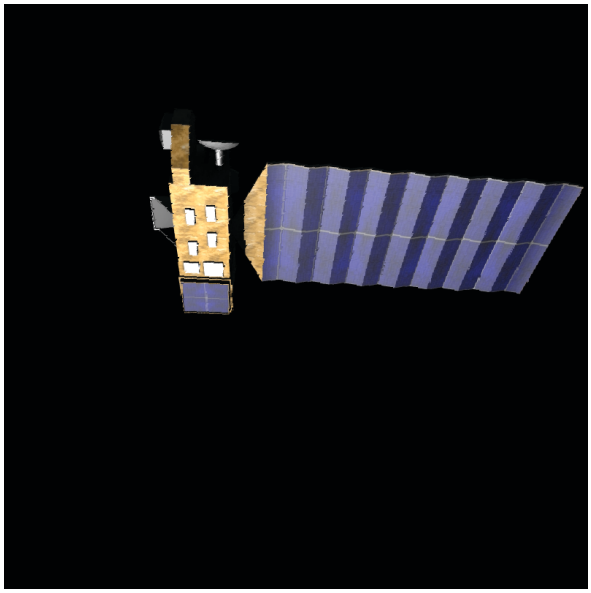

Figure 9. Warped image

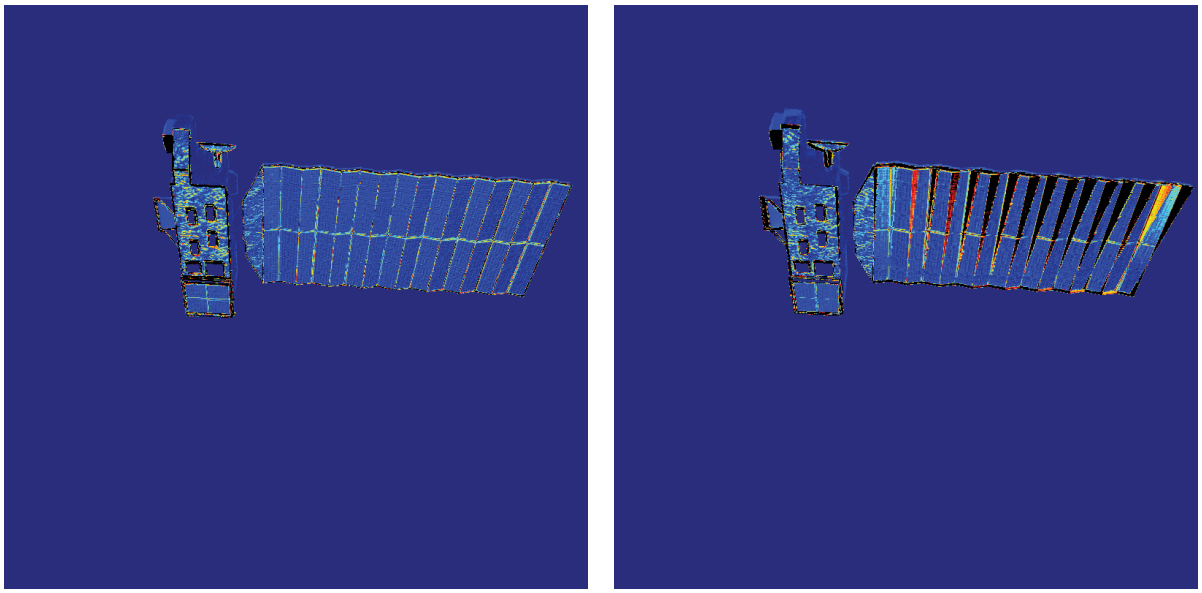

(a) Manual warped difference image $I_1 - I_2$ (b) Automatic warped difference image $I_1 - I_2$

Figure 10. Comparison of difference images

The warped version of I_1 is given in Figure 9. Again, the box is visible in the image. The difference image between I_2 and the warped image I_w is given in Figure 10(b). For ease of comparison between the manual and automatic results, the difference image generated using manually selected correspondence points from Figure 5(b) has been repeated as Figure 10(a). The automatically found correspondence points generated a noisy difference image with stronger homography errors.

Due to the increased amount of homography error, a more aggressive morphological filter was needed. A ball-shaped structuring element with a radius of seven pixels was used to generate the eroded difference image in Figure 11(a). Applying Otsu's method and thresholding produces the change detection result in Figure 11(b). Again, the algorithm has detected the loss of the box on the upper corner of the satellite.

(a) Eroded warped difference image (b) Change detection result

Figure 11. Removal of homography errors

5. RESULTS

The homography based change detector is much less sensitive to changes in pose than ordinary image differencing, as shown in Figure 5. A large change in pose which exposes a previously unobserved side of the RSO will be detected as a change. This is desirable, since an image containing a view of a different side of the RSO can be considered new information which should be flagged.

The homography-based change detector is not illumination invariant. Changes in the lighting, such as new shadows or specular reflections, will be flagged as changes. This would cause the algorithm to generate false positives unless care is taken to select a base image taken under the same lighting conditions. Since the location of the inspector, the sun, and the RSO are all known from their ephemerides, it would be possible to only compare images if all of these objects are in similar locations. This could be accomplished by building a database of base inspection images under many lighting conditions, and then comparing the comparison image to the base image with the most similar lighting characteristics.

If the RSOs are in geosynchronous or sun synchronous orbits, placing the inspection satellite in a sun synchronous orbit would ensure that the lighting conditions are the same during each inspection. However, since sun synchronous orbits have an altitude of just 600–800 km, detailed inspection of objects in geosynchronous orbit with altitudes of nearly 36,000 km would be difficult.

Although the SIFT produces noisier correspondence points than manual selection, the points that it produces are sufficient for moderate changes in pose. However, changes of pose that exceed 15–20 degrees frequently result in no pairs of correspondence points being returned by Lowe's algorithm.

REFERENCES

[1] Shoemaker, J., "Space situational awareness and mission protection," *DARPATech*, 208–211 (2005).

[2] Ma, Y., Soatto, S., Košecká, J., and Sastry, S. S., [*An Invitation to 3-D Vision*], vol. 26, Springer (2006).

[3] Lowe, D. G., "Distinctive image features from scale-invariant keypoints," *International Journal of Computer Vision* **60**(2), 91–110 (2004).

[4] Vedaldi, A. and Fulkerson, B., "VLFeat: An open and portable library of computer vision algorithms." `http://www.vlfeat.org/` (2008).

[5] Otsu, N., "A threshold selection method from gray-level histograms," *IEEE Transactions on Systems, Man and Cybernetics* **9**, 62–66 (January 1979).

[6] National Aeronautics and Space Administration, "3D models." `http://www.nasa.gov/multimedia/3d_resources/models.html`.